

RISM: Single-Modal Image Registration via Rank-Induced Similarity Measure

Aboozar Ghaffari and Emad Fatemizadeh, *Member, IEEE*

Abstract—Similarity measure is an important block in image registration. Most traditional intensity-based similarity measures (e.g., sum-of-squared-difference, correlation coefficient, and mutual information) assume a stationary image and pixel-by-pixel independence. These similarity measures ignore the correlation between pixel intensities; hence, perfect image registration cannot be achieved, especially in the presence of spatially varying intensity distortions. Here, we assume that spatially varying intensity distortion (such as bias field) is a low-rank matrix. Based on this assumption, we formulate the image registration problem as a nonlinear and low-rank matrix decomposition (NLLRMD). Therefore, image registration and correction of spatially varying intensity distortion are simultaneously achieved. We illustrate the uniqueness of NLLRMD, and therefore, we propose the rank of difference image as a robust similarity in the presence of spatially varying intensity distortion. Finally, by incorporating the Gaussian noise, we introduce rank-induced similarity measure based on the singular values of the difference image. This measure produces clinically acceptable registration results on both simulated and real-world problems examined in this paper, and outperforms other state-of-the-art measures such as the residual complexity approach.

Index Terms—Image registration, spatially varying intensity distortion, low-rank matrix, singular-value decomposition.

I. INTRODUCTION

IMAGE registration, the spatially varying alignment of two images, is an important pre-process in many applications, e.g., remote sensing [1], computer-assisted surgery [2], and medical image analysis and processing [3]. Two images may have different conditions such as imaging modality, time, and subject.

In the literature of image registration, two approaches have been proposed [4]. In the first approach, image features are used where the correspondence between the features or landmarks in the two images is the basis. The two main steps of this approach are features extraction and features matching between the two images. The features may be gradient, edge, geometric shape and contour, image skeleton, landmark [5], response of Gabor filter [6], response of alpha stable filter [7], or the intensity histogram [8]. The extraction of appropriate features plays a main role in obtaining successful registration.

Manuscript received August 8, 2014; revised January 17, 2015 and May 22, 2015; accepted September 1, 2015. Date of publication September 16, 2015; date of current version October 15, 2015. The associate editor coordinating the review of this manuscript and approving it for publication was Prof. David Frakes. (Corresponding author: Aboozar Ghaffari.)

The authors are with the Electrical Engineering Department, Sharif University of Technology, Tehran 11365-11155, Iran (e-mail: aboozar412@gmail.com; fatemizadeh@sharif.edu).

Color versions of one or more of the figures in this paper are available online at <http://ieeexplore.ieee.org>.

Digital Object Identifier 10.1109/TIP.2015.2479462

In the second approach, the intensity of images, the simplest features, is used to register the two images. In fact, the intensity similarity between the images is directly used. This class consists of three main modules: a similarity measure, a spatial transform (rigid or nonrigid), and an optimization algorithm.

Similarity measure plays a crucial role in the accuracy of intensity-based registration methods, especially in the presence of noise, outliers, bias field distortion, and spatially varying intensity distortion. Hence, defining an appropriate similarity measure is a challenging task in this regard. Traditional similarity measures are sum-of-squared-differences (SSD), correlation coefficient (CC), correlation ratio (CR) [9], and mutual information (MI) [10], [11]. Several modifications of these similarity measures, such as Bivariate CR combining intensity and gradient information [12], and Tsallis entropy [13], have been proposed. These traditional similarity measures basically assume pixel-by-pixel independence and image stationarity. These assumptions are used to analyze these measures from the maximum a posteriori (MAP) perspective [14]. The random shuffling of pixels in the ROIs will not change the value of these similarities. In practice, however, spatially varying intensity distortion is present; hence, the assumptions are violated, and registration by these similarity measures is not robust. Also, real images often suffer from spatially varying intensity distortion, for example, magnetic resonance imaging (MRI) may often be corrupted by slow-varying intensity bias fields [15], or visual-band images may suffer from illumination non-homogeneity and reflectance artifacts [16] and illumination variations in geometric images [17]. To overcome the spatially varying intensity distortion, two categories of registration methods are proposed: simultaneous intensity correction and registration, and the use of an appropriate model of distortion.

In the first category, the methods try to compensate the spatially varying intensity distortion. Hence, image registration is done after the correction. The works of [18] and [19] use this idea. Complexity and time consumption are two major problems in this category.

In the second category, in order to model the spatially varying intensity distortion, a robust similarity measure is basically defined. The intensity spatial dependencies are dealt with using an appropriate model. Some methods use complicated probabilistic models such as Markov random fields (MRF) and MAP-MRF [20], [21]. One group of methods use the simplest models, by assuming constant spatially varying intensity distortion within a small neighborhood around each pixel. Two similarity measures of Regional Mutual

Information (RMI) [15] and conditional MI (cMI) [22] are defined based on the local evaluation of MI. Locally evaluated MI in combination with standard global MI was also used [23]. Numerous local minima of the objective function and also the size of the local region are the problems of these methods. In another study, spatially varying intensity distortion is modeled by sparse representation in the transform domain, and image registration is achieved by minimizing the sparseness of the difference image in the transform domain [24]. An effective similarity measure in the presence of spatially varying intensity distortion is Residual Complexity (RC) [25], [26]. This measure uses the probability density function of $\exp(-\lambda \|\mathbf{PS}\|^2)$ to model spatially varying intensity distortion (S), where \mathbf{P} is a linear operator. RC measures the compression complexity (sparseness) of the residual image between the two registered images in the discrete cosine transform (DCT) domain.

Recently, low-rank matrix recovery has become a popular tool in signal and image processing and control theory [27]–[31]. In these applications, the problem is to find a matrix $\mathbf{S} \in \mathbb{R}^{n \times m}$ with minimum rank $r \ll \min(n, m)$, subject to linear constraints $\mathbf{y} = A(\mathbf{S}) \in \mathbb{R}^b$, i.e. a low-rank recovery problem:

$$\min_{\mathbf{S}} \text{rank}(\mathbf{S}) \quad s.t. \quad \mathbf{y} = A(\mathbf{S}) \quad (1)$$

where $A : \mathbb{R}^{n \times m} \rightarrow \mathbb{R}^b$ is a linear operator. In this paper, we model spatially varying intensity distortion with a low-rank matrix to define a robust similarity measure in the presence of this distortion. To our best knowledge, using this model is new in image registration. To compensate for this distortion, we introduce a new low-rank matrix recovery which is called nonlinear and low-rank matrix decomposition (NLLRMD). The goal of the approach is to find a low-rank matrix subject to a nonlinear constraint, which is dependent on the geometric transform. The nonlinear constraint of the proposed problem is the main difference with respect to the problem as expressed by (1). Based on NLLRMD, spatially varying intensity correction and registration are simultaneously performed. This registration method is closely related to both categories mentioned above. In this approach, the content of non-stationary intensity distortion is separated from floating and reference images. We will illustrate the uniqueness of this decomposition model. Then, we suggest a similarity measure based on the rank of the difference image. We call it rank-induced similarity measure (RISM).

The rest of this paper is organized as follows. Section II provides the main idea, and a new similarity measure is introduced based on the matrix rank. At first, image registration is stated based on NLLRMD. Then, the uniqueness of NLLRMD is discussed. Finally, Gaussian noise is included in the definition of the new similarity measure. Section III provides experimental results that demonstrates the effectiveness of our method and compares its performance with that of RC, MI, and SSD approaches. Finally, in Section IV, we conclude and point out future work direction image.

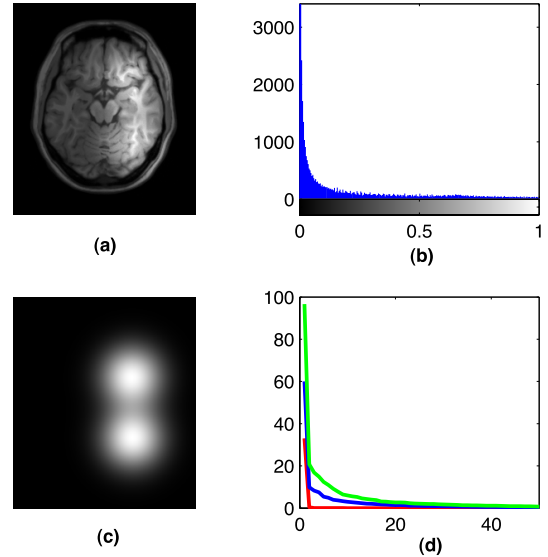


Fig. 1. (a) and (c) MRI image with spatially varying intensity distortion and Bias field, respectively; (b) Distribution of spatially-varying intensity distortion; (d) Singular values of spatially-varying intensity distortion (red) and original image without bias field (blue) and distorted image (green).

II. A MATHEMATICAL FRAMEWORK: THE MAIN IDEA AND THE PROPOSED METHOD

Consider two aligned images R and F , where R and F are the reference and floating images respectively, and assume the following intensity relationship in the matrix form:

$$\mathbf{R} = \mathbf{F}(T_{op}) + \mathbf{S}_{op} + \eta \quad (2)$$

where T_{op} is an optimum transform for registering the reference image $\mathbf{R} \in \mathbb{R}^{n \times m}$, and $\mathbf{F}(T_{op}) \in \mathbb{R}^{n \times m}$ is a floating image. $\eta \in \mathbb{R}^{n \times m}$ is the noise matrix with i.i.d. entries sampled from a zero mean Gaussian distribution with variance ν_n^2 . $\mathbf{S}_{op} \in \mathbb{R}^{n \times m}$ is a spatially varying intensity distortion such as the bias field. If $\mathbf{S}_{op} = 0$, SSD similarity measure is optimal from MAP point of view [14]. As spatially varying intensity distortion has pixel-by-pixel dependency, and also its intensity distribution is non-Gaussian, SSD is not a robust similarity measure in the presence of this distortion. To overcome this, we propose a new similarity measure based on low-rank matrix recovery. It is assumed that spatially varying intensity distortion is a low-rank matrix.

To illustrate the low-rank matrix assumption of spatially varying intensity distortion, Fig. 1 presents an example of a spatially varying intensity distortion. Spatially varying intensity distortion is modeled by the Gaussian mixture. Fig. 1(b) shows the intensity histogram of spatially varying intensity distortion. Obviously, this distribution is not Gaussian. Fig. 1(d) shows singular values of spatially varying intensity distortion and floating image. It is observable that the singular values of spatially varying intensity distortion are compact. This is our main idea for a new similarity measure. In fact, we suppose that the noise or distortion has two terms in the model (2). The first is spatially varying intensity distortion, which has a low-rank matrix form, and the second term is the popular model of Gaussian noise.

Next, by considering only the first term, correction of spatially varying intensity distortion and image registration are combined by the new model of nonlinear and low-rank matrix decomposition. Using this, the rank of the difference image is introduced as a new similarity measure in the presence of spatially varying intensity distortion. Then, with respect to the relation of ℓ_2 norm and singular values, RISM is introduced as a new similarity measure which is a combination of ℓ_0 and ℓ_2 norms of singular values of the difference image.

A. Image Registration: Nonlinear and Low-Rank Matrix Decomposition

Here, for simplicity, we assume first that the Gaussian noise is not present. Towards the end of this section, the effect of Gaussian noise in the new similarity measure will be considered. Now, (2) is reduced to

$$\mathbf{R} = \mathbf{F}(T_{op}) + \mathbf{S}_{op} \quad (3)$$

Our main idea is to decompose the reference image \mathbf{R} into floating image $\mathbf{F}(T) \in \mathbb{R}^{n \times m}$ and a spatially varying intensity distortion $\mathbf{S} \in \mathbb{R}^{n \times m}$. Each entry of $\mathbf{F}(T)$ is nonlinear in terms of the parameters of geometric transform T . The registration model can be a nonrigid or rigid transform. We assume that nonstationary intensity distortion \mathbf{S}_{op} is a low-rank matrix i.e., $\text{rank}(\mathbf{S}_{op}) = r$ where $r \ll \min\{n, m\}$.

Following the above discussion, we propose the NLLRMD problem:

$$(NLLRMD): \hat{T}, \hat{\mathbf{S}} = \underset{T, \mathbf{S}}{\operatorname{argmin}} \text{rank}(\mathbf{S}) \quad \text{s.t. } \mathbf{R} = \mathbf{F}(T) + \mathbf{S} \quad (4)$$

NLLRMD problem states that image registration and spatially varying correction are simultaneously achieved considering the assumption of a low-rank matrix. The nonlinear constraint $\mathbf{R} = \mathbf{F}(T) + \mathbf{S}$ is the main difference of our problem with traditional low-rank matrix recovery (1).

To solve NLLRMD, the following important questions are raised that must be answered positively.

- 1) **Uniqueness:** Does the NLLRMD problem have a unique solution, $\hat{T} = T_{op}$?
- 2) **Practical Solver:** Does the optimization problem of NLLRMD have a practical solver, which will be robust against Gaussian noise?

In the rest of this section, we will answer these questions.

In summary, by introducing the new model of matrix decomposition, we propose the robust similarity measure $\text{rank}(\mathbf{R} - \mathbf{F}(T))$ in the presence of spatially varying intensity distortion.

B. Uniqueness

The main objective of this subsection is to show the uniqueness of NLLRMD, meaning that there exist unique matrices \mathbf{S}_{op} and $\mathbf{F}(T_{op})$, satisfying (3). However, if there are multiple decompositions of \mathbf{R} into $\mathbf{F}(T) + \mathbf{S}$ with low-rank \mathbf{S} and nonlinear $\mathbf{F}(T)$, there would be no hope of a perfect image registration.

Let $\mathbf{U}\Sigma\mathbf{V}^T$ denote the singular-value decomposition (SVD) of \mathbf{S}_{op} , and consider the following subspaces:

- 1) $\Phi(\mathbf{S}_{op}) = \{\mathbf{Z} \in \mathbb{R}^{n \times m} : \mathbf{Z} = \mathbf{U}\mathbf{W}_1^T + \mathbf{W}_2\mathbf{V}^T, \mathbf{W}_1 \in \mathbb{R}^{r \times m}, \mathbf{W}_2 \in \mathbb{R}^{r \times n}\}$, containing the column or row space of \mathbf{S}_{op} . In fact, subspace $\Phi(\mathbf{S}_{op})$ represents the space of spatially varying intensity distortions of rank r .
- 2) $\Omega(T_{op}) = \{\mathbf{Z} : \mathbf{Z} = \mathbf{F}(T_{op}) - \mathbf{F}(T), \forall T\}$, representing the difference matrix space between $\mathbf{F}(T)$ and $\mathbf{F}(T_{op})$. Considering $\mathbf{F}(T) \neq \mathbf{F}(T_{op}), \forall T \neq T_{op}$, perfect registration is equivalent to $\mathbf{Z} = \mathbf{0} \in \mathbb{R}^{n \times m}$, obtained only when $T = T_{op}$. On the other hand, the subspace $\Omega(T_{op})$ represents the alignment between $\mathbf{F}(T)$ and $\mathbf{F}(T_{op})$. The subspace $\Omega(T_{op})$ is dependent on the geometric transform and floating image.

In the absence of a spatially varying intensity distortion ($\mathbf{S}_{op} = \mathbf{0}$), if $\mathbf{F}(T) \neq \mathbf{F}(T_{op}), \forall T \neq T_{op}$, it is obvious that T_{op} is the unique geometric transform by NLLRMD. This simple example may be stated from matrix subspace viewpoint. $\mathbf{S}_{op} = \mathbf{0}$ means that the matrix subspace $\Phi(\mathbf{S}_{op})$ contains only the origin. Also, $\mathbf{F}(T) \neq \mathbf{F}(T_{op}), \forall T \neq T_{op}$ means that the matrix subspace $\Omega(T_{op})$ contains the origin only when $T = T_{op}$. Therefore the intersection of these matrix subspaces contains only the origin. We use this concept for illustrating the uniqueness of NLLRMD.

First, let's assume that the subspace $\Phi(\mathbf{S}_{op})$ is known. The following theorem states the necessary and sufficient conditions guaranteeing the unique decomposability of \mathbf{R} .

Theorem 1: Suppose $\Phi(\mathbf{S}_{op})$ is known. Matrix \mathbf{R} is uniquely decomposed into $\mathbf{F}(T_{op}) + \mathbf{S}_{op}$ if and only if $\Omega(T_{op}) \cap \Phi(\mathbf{S}_{op}) = \{\mathbf{0} \in \mathbb{R}^{n \times m}\}$, and $\mathbf{F}(T) \neq \mathbf{F}(T_{op}), \forall T \neq T_{op}$.

Proof: Assume, on the contrary, that there exists a matrix \mathbf{S} satisfying $\mathbf{R} = \mathbf{F}(T) + \mathbf{S}$, $\mathbf{S} \neq \mathbf{S}_{op}$ and $\mathbf{S} \in \Phi(\mathbf{S}_{op})$. Then, $\mathbf{Z} = \mathbf{F}(T_{op}) - \mathbf{F}(T) = \mathbf{S} - \mathbf{S}_{op}$, a nonzero matrix, is an intersection matrix of the subspaces $\Omega(T_{op})$ and $\Phi(\mathbf{S}_{op})$, which is a contradiction.

Conversely, on the contrary, suppose that there exists a nonzero $\mathbf{Z} \in \Omega(T_{op}) \cap \Phi(\mathbf{S}_{op})$. Since $\mathbf{Z} = \mathbf{F}(T_{op}) - \mathbf{F}(T)$, then $\mathbf{S} = \mathbf{S}_{op} + \mathbf{Z} \in \Phi(\mathbf{S}_{op})$ is a feasible solution, satisfying $\mathbf{R} = \mathbf{F}(T) + \mathbf{S}$. This contradicts the uniqueness assumption. The condition $\mathbf{F}(T) \neq \mathbf{F}(T_{op}), \forall T \neq T_{op}$ ensures that $\mathbf{Z} = \mathbf{0} \in \Omega(T_{op}) \cap \Phi(\mathbf{S}_{op})$ only when $T = T_{op}$. ■

As the subspace $\Phi(\mathbf{S}_{op})$ is known, theorem 1 states that the decomposition of \mathbf{R} is locally unique. Note that the low-rank assumption has a main role in this theorem. For example, if \mathbf{S}_{op} is of full rank, then $\Omega(T_{op}) \cap \Phi(\mathbf{S}_{op}) = \Omega(T_{op})$, which contradicts the theorem condition; hence, we have many decompositions. However, theorem 1 does not say how this unique solution is determined. Here, we use the low-rank assumption to obtain the unique decomposition. So, in the rest of this section, we illustrate the uniqueness of NLLRMD problem.

Before stating the uniqueness theorem, we give an important definition, which is a key property for our study of uniqueness.

Definition 1: k-intersection Constant of nonlinear matrix $\mathbf{F}(T_{op})$ (ICN) is defined to be the smallest number $\delta_k(T_{op})$ such that

$$(1 - \delta_k(T_{op}))\|\mathbf{F}(T_{op}) - \mathbf{F}(T)\|_F^2 \leq \|\mathbf{F}(T_{op}) - \mathbf{F}(T) - \mathbf{X}_k\|_F^2 \quad (5)$$

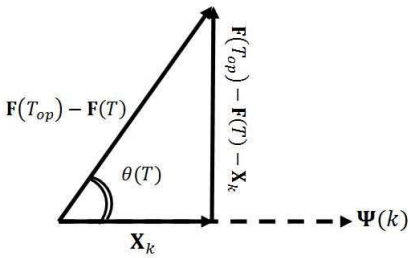


Fig. 2. Geometric representation of k-intersection Constant of nonlinear matrix $\mathbf{F}(T_{op})$ (ICN).

holds for each geometric transform ($\forall T$) where $\mathbf{X}_k = \text{argmin}_{\text{rank}(\mathbf{X}) \leq k} \|\mathbf{F}(T_{op}) - \mathbf{F}(T) - \mathbf{X}\|_F^2$.

In the above equation $\|\mathbf{X}\|_F = \sqrt{\sum_{i,j} x_{ij}^2}$ is the Frobenius norm. The constant $\delta_k(T_{op})$ measures the intersection between the subspaces $\Psi(k) = \{\mathbf{X} \in \mathbb{R}^{n \times m} : \text{rank}(\mathbf{X}) \leq k\}$ and $\Omega(T_{op})$.

ICN definition has a geometric representation, illustrated in Fig. 2. Suppose the geometric transform T is fixed, and $\mathbf{U}_T \Sigma_T \mathbf{V}_T$ is SVD of $\mathbf{F}(T_{op}) - \mathbf{F}(T)$ with singular values $\tau_1 \geq \tau_2 \geq \dots \geq \tau_{\min(n,m)}$. Using the classical Eckart-Young-Mirsky theorem [32], [33], \mathbf{X}_k is given by a truncated singular-value decomposition of $\mathbf{F}(T_{op}) - \mathbf{F}(T)$, i.e., $\mathbf{X}_k = \mathbf{U}_T \Sigma_{Tk} \mathbf{V}_T$ where the first k diagonal entries of Σ_{Tk} are the largest k singular values of Σ_T , and the rest of the entries are zero. From Fig. 2, we have

$$\begin{aligned} \sin^2(\theta(T)) &= \frac{\|\mathbf{F}(T_{op}) - \mathbf{F}(T) - \mathbf{X}_k\|_F^2}{\|\mathbf{F}(T_{op}) - \mathbf{F}(T)\|_F^2} \\ &= \frac{\sum_{i=1}^r \tau_i^2}{\sum_{i=1}^{\min(n,m)} \tau_i^2}. \end{aligned} \quad (6)$$

From the ICN definition, we will have $\delta_k(T_{op}) \geq \cos^2(\theta(T))$; hence,

$$\delta_k(T_{op}) = \max_T \cos^2(\theta(T)) \quad (7)$$

It is evident that ICN illustrates the minimum angle between the subspaces $\Psi(k)$ and $\Omega(T_{op})$. The range of $\delta_k(T_{op})$ is $[0, 1]$. The upper bound is attained when $\Psi(k) \cap \Omega(T_{op})$ contains a nonzero element. The condition $\delta_k(T_{op}) < 1$ implies $\Psi(k) \cap \Omega(T_{op}) = \{\mathbf{0} \in \mathbb{R}^{m \times n}\}$; Therefore, two matrix subspaces $\Psi(k)$ and $\Omega(T_{op})$ intersect only at the origin.

Now, using the ICN, we present the following uniqueness theorem:

Theorem 2 (Uniqueness - ICN): Suppose $\delta_{2r}(T_{op}) < 1$ and $\mathbf{F}(T) \neq \mathbf{F}(T_{op}), \forall T \neq T_{op}$, then, matrix \mathbf{R} is uniquely decomposed into $\mathbf{R} = \mathbf{F}(T_{op}) + \mathbf{S}_{op}$ by NLLRMD.

Proof: Assume, on the contrary, that there exists a matrix \mathbf{S} of rank at most r , satisfying $\mathbf{R} = \mathbf{F}(T) + \mathbf{S}$ and $\mathbf{S} \neq \mathbf{S}_{op}$. The condition $\mathbf{F}(T) \neq \mathbf{F}(T_{op}), \forall T \neq T_{op}$ ensures that $T = T_{op}$ only when $\mathbf{S} = \mathbf{S}_{op}$. Then, $\mathbf{X} = \mathbf{S} - \mathbf{S}_{op}$ is a nonzero matrix of rank at most $2r$, and $\mathbf{F}(T_{op}) - \mathbf{F}(T) - \mathbf{X} = 0$; hence, $\mathbf{X}_{2r} = \mathbf{X}$. From ICN definition, we have $0 < (1 - \delta_{2r}(T_{op})) \|\mathbf{F}(T_{op}) - \mathbf{F}(T)\|_F^2 \leq \|\mathbf{F}(T_0) - \mathbf{F}(T) - \mathbf{X}_{2r}\|_F^2 = 0$, which is a contradiction. \blacksquare

When floating image $\mathbf{F}(T)$ has more complexity than the spatial intensity distortion, and \mathbf{S}_{op} is of low rank, we can expect that the condition $\delta_{2r}(T_{op}) < 1$ is satisfied.

In the above discussion, we illustrated the uniqueness via the intersection of two subspaces. In other words, \mathbf{R} is uniquely decomposed when the intersection of two matrix subspaces (low-rank and nonlinear subspaces) has only zero elements. The condition of theorem 2 is the worst case and contains the least information about \mathbf{S}_{op} . This condition is totally related to the image registration model $\mathbf{F}(T)$ via ICN definition. An advantage of ICN is that $\delta_{2r}(T_{op})$ can be computed without knowing the matrix subspace of $\Phi(\mathbf{S}_{op})$.

We now define the new subspace of $\Omega(T_{op}, k)$:

$$\Omega(T_{op}, k) = \{\mathbf{Z} : \mathbf{Z} = \mathbf{F}(T_{op}) - \mathbf{F}(T), \text{rank}(\mathbf{Z}) < k, \forall T\} \quad (8)$$

where $\Omega(T_{op}, k) \subset \Omega(T_{op}) = \Omega(T_{op}, \min(n, m))$. It is obvious that $\delta_{2r}(T_{op}) < 1$ is equivalent to $\Omega(T_{op}, 2r) = \{\mathbf{0} \in \mathbb{R}^{n \times m}\}$. Here, we suppose that $\delta_{2r}(T_{op}) = 1$ or the subspace $\Omega(T_{op}, 2r)$ has nonzero element. Now, we explain the uniqueness of NLLRMD problem via the properties of rank. Before stating the uniqueness theorem, we restate the following property about the rank of the summation matrix [34].

Let $\mathbf{V}(\mathbf{A})$ and $\mathbf{V}(\mathbf{B})$ be the column spaces of \mathbf{A} and $\mathbf{B} \in \mathbb{R}^{n \times m}$ respectively, and let $\mathbf{V}(\mathbf{A}^T)$ and $\mathbf{V}(\mathbf{B}^T)$ be the row spaces of \mathbf{A} and \mathbf{B} respectively. Now suppose \mathbf{A} and \mathbf{B} are two matrices of the same size, and

$$\begin{aligned} e &= \text{dimension}(\mathbf{V}(\mathbf{A}) \cap \mathbf{V}(\mathbf{B})) \\ d &= \text{dimension}(\mathbf{V}(\mathbf{A}^T) \cap \mathbf{V}(\mathbf{B}^T)) \end{aligned} \quad (9)$$

where $\text{dimension}(\cdot)$ denotes the dimension of vector space. Then the upper and lower bounds of $\text{rank}(\mathbf{A} + \mathbf{B})$ will be

$$\begin{aligned} \text{rank}(\mathbf{A} + \mathbf{B}) &\leq \text{rank}(\mathbf{A}) + \text{rank}(\mathbf{B}) - \max(e, d) \\ \text{rank}(\mathbf{A} + \mathbf{B}) &\geq \text{rank}(\mathbf{A}) + \text{rank}(\mathbf{B}) - e - d \end{aligned} \quad (10)$$

and $\text{rank}(\mathbf{A} + \mathbf{B}) = \text{rank}(\mathbf{A}) + \text{rank}(\mathbf{B})$ if and only if $e = d = 0$ [34].

The following Theorem states the sufficient conditions of uniqueness when $\delta_{2r}(T_{op}) = 1$.

Theorem 3: Suppose

$$\begin{aligned} \forall \mathbf{A} &\in \Omega(T_{op}, 2r) \\ e &= \text{dimension}(\mathbf{V}(\mathbf{A}) \cap \mathbf{V}(\mathbf{S}_{op})) = 0 \\ d &= \text{dimension}(\mathbf{V}(\mathbf{A}^T) \cap \mathbf{V}(\mathbf{S}_{op}^T)) = 0 \end{aligned} \quad (11)$$

and, $\mathbf{F}(T) \neq \mathbf{F}(T_{op}), \forall T \neq T_{op}$. Then matrix \mathbf{R} is uniquely decomposed into $\mathbf{R} = \mathbf{F}(T_{op}) + \mathbf{S}_{op}$ by NLLRMD.

Proof: For simplicity, define $\mathbf{A} = \mathbf{F}(T_{op}) - \mathbf{F}(T)$ and $\mathbf{B} = \mathbf{S}_{op}$. Then we have $\text{rank}(\mathbf{R} - \mathbf{F}(T)) = \text{rank}(\mathbf{A} + \mathbf{B})$. With respect to the subspace $\Omega(T_{op}, 2r)$, we consider the following two cases:

- 1) $\mathbf{A} \notin \Omega(T_{op}, 2r)$ or $\text{rank}(\mathbf{A}) \geq 2r + 1$: It is obvious that the maximum of e and d is equal to r . Hence, from (10), the lower bound of $\text{rank}(\mathbf{A} + \mathbf{B})$ will be $r + 1$ in the worst case.
- 2) $\mathbf{A} \in \Omega(T_{op}, 2r)$ or $\text{rank}(\mathbf{A}) \leq 2r$: In this case, from the rank property and the assumptions of theorem ($e = d = 0$), we have $\text{rank}(\mathbf{A} + \mathbf{B}) = \text{rank}(\mathbf{A}) + \text{rank}(\mathbf{B}) = \text{rank}(\mathbf{A}) + r$.

From these two cases, it is obvious that the global minimum of $\text{rank}(\mathbf{A} + \mathbf{B})$ is obtained when $\mathbf{A} = \mathbf{F}(T_{op}) - \mathbf{F}(T) = \mathbf{0}$. The condition $\mathbf{F}(T) \neq \mathbf{F}(T_{op}), \forall T \neq T_{op}$ ensures that $T = T_{op}$ is the optimum solution of NLLRMD; Therefore, perfect registration is obtained. ■

Theorem 3 gives the uniqueness condition via the intersection of two subspaces \mathbf{S}_{op} and $\Omega(T_{op}, 2r)$. This theorem is an extension of theorem 2.

In summary, we proved the sufficient and necessary conditions of the unique decomposition when we know the matrix subspace of spatially varying intensity distortion, without considering the method of decomposition. As \mathbf{S}_{op} is a low-rank matrix ($\text{rank}(\mathbf{S}_{op}) \ll \min(n, m)$), we propose to use NLLRMD problem as a method of decomposition. Next, we illustrate the uniqueness conditions for this problem.

C. RISM: Rank Induced Similarity Measure

Following the previous subsections, the rank of the difference image $\mathbf{R} - \mathbf{F}(T)$ is proposed as a similarity measure in the presence of the spatially varying intensity distortion. Here, as in (2), the effect of Gaussian noise is considered.

Let $\mathbf{R} - \mathbf{F}(T) = \mathbf{U}\Sigma\mathbf{V}^T$ be SVD of $\mathbf{R} - \mathbf{F}(T)$ where $\Sigma = \text{diag}\{\sigma_1, \sigma_2, \dots, \sigma_{\min(n,m)}\}$. σ_i is the i^{th} singular value of $\mathbf{R} - \mathbf{F}(T)$ where $\sigma_1 \geq \sigma_2 \geq \dots \geq \sigma_{\min(n,m)} \geq 0$. The rank and singular values are related as follows:

$$\text{rank}(\mathbf{R} - \mathbf{F}(T)) = \sum_{i=1}^{\min(n,m)} \sigma_i^0 = \|\sigma\|_0 \quad (12)$$

where $\sigma = [\sigma_1, \sigma_2, \dots, \sigma_{\min(n,m)}]^T \in \mathbb{R}^{\min(n,m)}$, and $\|\sigma\|_0$ denotes for the ℓ^0 norm of σ , that is, the number of nonzero singular values.

In the presence of Gaussian noise, the i^{th} singular value of $\mathbf{R} - \mathbf{F}(T)$ with $i > r = \text{rank}(\mathbf{S}_{op})$ is not necessarily zero. Hence, with respect to the sensitivity of the ℓ^0 norm to noise, (12) is unstable and not appropriate. To solve this problem, we determine the rank by the number of significant (large) singular values. To do this, the following definition is used as the effective rank of a perturbed matrix in [35].

Definition 2 (Effective Rank [35]): Suppose that $\mathbf{E} \in \mathbb{R}^{n \times m}$ is a noise (perturbation) matrix, then for any matrix $\mathbf{B} = \mathbf{A} + \mathbf{E} \in \mathbb{R}^{n \times m}$ which is a perturbed matrix of $\mathbf{A} \in \mathbb{R}^{n \times m}$ with singular values $\beta_1 \geq \beta_2 \geq \dots \geq \beta_{\min(n,m)} > 0$, the effective rank is defined to be r , when

$$\beta_r > \epsilon_1 \geq \beta_{r+1} \quad (13)$$

where $1 \leq r \leq \min(r, m)$ and ϵ_1 is the largest singular value of \mathbf{E} .

The following theorem provides a sufficient condition for the equality of the effective rank of \mathbf{B} and the rank of \mathbf{A} .

Theorem 4 [35]: Suppose $\mathbf{A} \in \mathbb{R}^{n \times m}$ is a matrix of rank r , where $r \leq \min(n, m)$ with singular values $\alpha_1 \geq \alpha_2 \geq \dots \geq \alpha_r > 0$, and \mathbf{B} and \mathbf{E} are $n \times m$ matrices, as defined in the definition of effective rank, with the largest singular value of \mathbf{E} denoted by ϵ_1 . If $\alpha_r > 2\epsilon_1$, then $\beta_r > \epsilon_1 \geq \beta_{r+1}$, and \mathbf{B} is said to have the effective rank of r .

The following lemma shows that the condition of theorem 4 is satisfied with high probability in the presence of low Gaussian noise. Before stating the lemma, we restate the following probability property of the largest singular value $\sigma_{\max}(\mathbf{Y})$ of Gaussian matrix \mathbf{Y} . Let $\mathbf{Y} \in \mathbb{R}^{n \times m}$ with $n \geq m$, and the distribution of its entries be zero mean Gaussian with variance $1/n$. Then the following inequality is proved in [36] for any $s > 0$

$$\text{prob}\{\sigma_{\max}(\mathbf{Y}) > 1 + \sqrt{m/n} + s\} \leq e^{-ns^2}. \quad (14)$$

Now, we will obtain a lower bound for the probability $\text{prob}\{\epsilon_1 < \alpha_r/2 | \alpha_r\}$ as follows:

Lemma 1: Let \mathbf{E} be an $n \times m$ matrix, as defined above, with $n \geq m$, and with i.i.d. entries sampled from the normal distribution with mean zero and variance v_n^2 , and $\lambda = \alpha_r/2v_n - \sqrt{n} - \sqrt{m} > 0$, then $\text{prob}\{\epsilon_1 < \alpha_r/2 | \alpha_r\} \geq 1 - e^{-\lambda^2/2}$.

Proof: Let $\mathbf{Y} = 1/\sqrt{nv_n^2}\mathbf{E}$ be an $n \times m$ matrix with $N(0, 1/n)$ entries. With respect to $\sigma_{\max}(\mathbf{Y}) = 1/\sqrt{nv_n^2}\epsilon_1$ and the inequality (14), we have

$$\text{prob}\{\epsilon_1 > v_n\sqrt{n} + v_n\sqrt{m} + sv_n\sqrt{n}\} \leq e^{-ns^2}.$$

As $\text{prob}\{\epsilon_1 < \alpha_r/2 | \alpha_r\} = 1 - \text{prob}\{\epsilon_1 > \alpha_r/2 | \alpha_r\}$ and defining $\alpha_r/2 = v_n\sqrt{n} + v_n\sqrt{m} + sv_n\sqrt{n}$, the proof is completed. ■

Therefore from the above lemma, it is obvious from the lower bound of $\text{prob}\{\epsilon_1 < \alpha_r/2 | \alpha_r\}$ that the condition of theorem 4 is satisfied with high probability when variance v_n^2 is small; In the other word, $\alpha_r/2v_n \gg \sqrt{n} + \sqrt{m}$. As in practice, the singular values of \mathbf{A} and \mathbf{E} are not known, in [35], the following upper and lower bounds on ϵ_1

$$\sqrt{cv_n} \leq \epsilon_1 \leq \sqrt{nm}v_n \quad (15)$$

are derived in terms of the theory of statistical significance test, where c is a function of the level of significance.

Here, we use the concept of effective rank of $\mathbf{B} = \mathbf{R} - \mathbf{F}(T)$ for a new similarity measure. In fact, in our formulation, $\mathbf{A} = \mathbf{F}(T_{op}) - \mathbf{F}(T) + \mathbf{S}_{op}$ is the low-rank matrix, and $\mathbf{E} = \eta$ is the perturbation matrix. From the effective rank viewpoint, a determined threshold by ϵ_1 is applied on the upper bound of sum operator in (12). Here, we set the threshold on the upper bound of (15). Therefore, the number (ℓ_0 norm) of significant singular values is calculated.

It is important to note that in our problem the Frobenius norm of $\mathbf{R} - \mathbf{F}(T)$ is an optimal similarity measure in the presence of only Gaussian noise [14]. The relation between the Frobenius norm and the singular values is $\|\mathbf{R} - \mathbf{F}(T)\|_F^2 = \sum_{i=1}^{\min(n,m)} \sigma_i^2$. On the other hand, the Frobenius norm is equivalent to the ℓ_2 norm of the singular values. To introduce a new similarity measure considering two noise models, we consider the following cases:

- 1) In the presence of spatially varying intensity distortion with the assumption of low rank, the ℓ_0 norm of singular values of $\mathbf{R} - \mathbf{F}(T)$ is an optimal similarity measure from the uniqueness viewpoint of NLLRMD.
- 2) In the presence of Gaussian noise, the ℓ_2 norm of singular values of $\mathbf{R} - \mathbf{F}(T)$ is an optimal similarity measure.

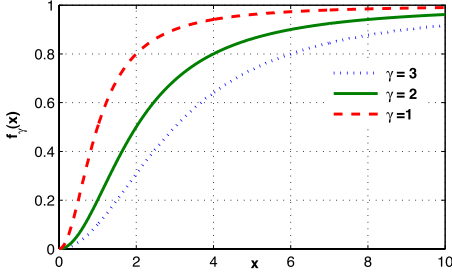


Fig. 3. Curve of $f_\gamma(x) = \frac{x^2}{x^2 + \gamma^2}$ with respect to x variable for different γ value.

- 3) In the presence of two types of noises, from the effective rank point of view, the singular values of $\mathbf{R} - \mathbf{F}(T)$ are divided into two parts of significant (large) and insignificant (small) singular values, which are related to the low rank and the Gaussian noise (perturbation) matrices, respectively.

From the above discussion, to define a robust similarity measure, we combine the ℓ_0 and ℓ_2 norms of singular values using the threshold found by the effective rank and the upper bound of (15). So, a similarity measure is defined by a weighted summation of the ℓ_0 norm of significant singular values and the ℓ_2 norm of insignificant singular values of $\mathbf{R} - \mathbf{F}(T)$. As the ℓ_0 norm and hard thresholding are not differentiable, we replace these with the following smooth function:

$$f_\gamma(x) = \frac{x^2}{x^2 + \gamma^2} \quad (16)$$

where γ is a constant and plays the role of thresholding as follows:

$$f_\gamma(x) \approx \begin{cases} 1; & \text{if } |x| \gg \gamma \\ \frac{x^2}{\gamma^2}; & \text{if } |x| \ll \gamma \end{cases} \quad (17)$$

On the other hand, we have the soft transient between two states of the ℓ_0 and ℓ_2 norms, classified by the found threshold of the effective rank.

The idea of a smooth function has been used before. The function (16) was used in the application of a robust estimator in the presence of outlier data [37]. In our application, the spatially varying intensity distortion has a role of outlier data in the domain of singular values. Recently, the idea of smooth function is the basis of the smoothed ℓ_0 norm method (SL0) [38], [39] for sparse recovery, and the smoothed rank function for matrix completion [40] and low-rank matrix recovery under affine constraints [41].

Fig. 3 shows $f_\gamma(x)$, for different γ values. It is clear that the transient is soft. In fact, $f_\gamma(x)$ is a function that combines the ℓ_0 and ℓ_2 norms. Hence, with respect to the above discussion, we propose rank induced similarity measure (RISM):

$$\begin{aligned} RISM(\mathbf{R}, \mathbf{F}) &= \sum_{i=1}^{\min(n,m)} f_\gamma(\sigma_i) = \sum_{i=1}^{\min(n,m)} \frac{\sigma_i^2}{\sigma_i^2 + \gamma^2} \\ \mathbf{R} - \mathbf{F}(T) &= \mathbf{U} \Sigma \mathbf{V}^T \\ \Sigma &= \text{diag}\{\sigma_1, \dots, \sigma_{\min(n,m)}\} \\ \gamma &= \max(1, \sqrt{nm} v_n) \end{aligned} \quad (18)$$

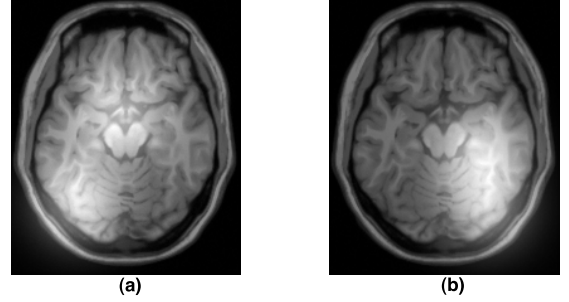


Fig. 4. (a) and (b) Floating and reference images used to compute the similarity measure functions.

where v_n^2 is the variance of the Gaussian noise or perturbation \mathbf{E} , as defined in Lemma 1. Because \mathbf{S}_{op} is not exactly the low-rank matrix, and also when $\gamma \rightarrow 0$, RISM is equal to the rank of $\mathbf{R} - \mathbf{F}(T)$ (ℓ_0 norm), which is not differentiable, the lower bound (one) has been considered for γ . Note that other forms for the smoothing functions, $f_\gamma(x)$, are also possible. Defining an appropriate smoothing function $f_\gamma(x)$ to achieve better performance of image registration is one task we will pursue further in our future study. Here, the noise variance v_n^2 is estimated from the wavelet coefficients of noisy image by the robust median estimator $v_n = \frac{\text{median}(|y_i|)}{0.6745}$, which is used from the finest scale wavelet coefficients ($y_i \in$ subband HH) [42].

To register two images R and $F(T)$, the optimization process of RISM is done iteratively to estimate the transform parameters using the gradient descent. An important part of the gradient computation is the gradient of RISM with respect to $\mathbf{R} - \mathbf{F}(T)$. Inspired by [40], this gradient is computed using the definition of the sub-differential [43]. A pseudo code to compute the similarity measure and its gradient may be as follows:

$$\begin{aligned} \mathbf{X} &= \mathbf{R} - \mathbf{F}(T); \\ \text{SVD: } \mathbf{X} &= \text{Udiag}\{\sigma_1, \dots, \sigma_{\min(n,m)}\} \mathbf{V}^T; \\ RISM(\mathbf{R}, \mathbf{F}) &= \sum_{i=1}^{\min(n,m)} f_\gamma(\sigma_i); \\ \frac{\partial RISM(\mathbf{X})}{\partial \mathbf{X}} &= \text{Udiag}\{f'_\gamma(\sigma_1), \dots, f'_\gamma(\sigma_{\min(n,m)})\} \mathbf{V}^T; \\ \nabla RISM &= -\frac{\partial RISM(\mathbf{X})}{\partial \mathbf{X}} \nabla \mathbf{F}(T) \frac{\partial T}{\partial \theta} \end{aligned} \quad (19)$$

where $\nabla \mathbf{F}$ is the intensity image gradient and θ denotes the transformation parameters. $f_\gamma(x)$ and $f'_\gamma(x)$ are $x^2/(x^2 + \gamma^2)$ and $2\gamma^2 x/(x^2 + \gamma^2)^2$, respectively.

III. EXPERIMENTAL RESULTS

In this paper, Free Form Deformation (FFD) with three hierarchical levels of B-spline control points [44] is used as a model of geometric transform. To optimize the transform parameters, the gradient descent is used iteratively. Here, the transformation regularization is applied for smoothness of space warping. This regularization is employed by the penalty term of distance between B-spline control points. In this

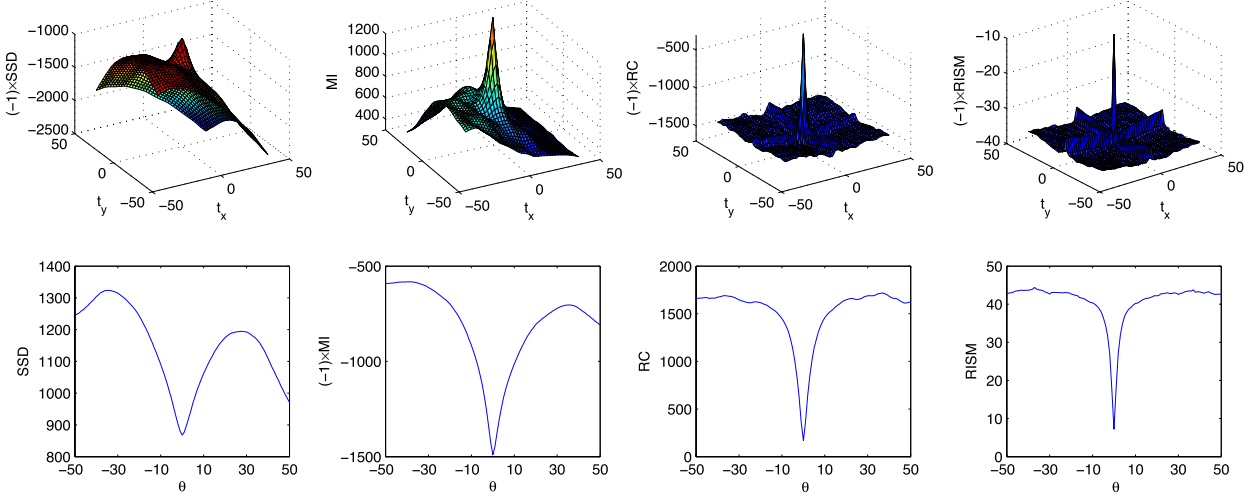


Fig. 5. Similarity measure functions of SSD, MI, RC, and our approach from left to right in aligning the images of Fig. 4. Top row: translation along the x and y axis; Bottom row: rotation only.

section, we performed nonrigid image registration experiments on both the simulated database obtained from BrainWeb [45] and real data to evaluate the proposed approach. The real data used are a video sequence of dynamic magnetic resonance imaging, a sequence of iris images, digital subtraction angiography (DSA), retina and LANDSAT satellite images. The performance of our similarity measure is also compared with SSD, RC, and MI similarity measures, which were implemented in Matlab, based on the Medical Image Registration Toolbox [25]. Here, we use SSD and MI as common similarity measures. Also, RC introduced recently simultaneously performs the correction of nonstationary intensity distortion and registration using MAP method.

In the rest of this section, first, we illustrate the robustness of the proposed similarity measure via its function with respect to the different geometric transform parameters. Then, the registration accuracy of different similarity measures is demonstrated via the simulated database in the presence of spatially varying intensity distortion and Gaussian noise. Finally, we test our measure using real data. All the experiments have been performed on a personal computer with Intel Core i7 2.2GHz and 8GB RAM.

A. Similarity Measure Functions

Here, the robustness of the proposed similarity measure in the presence of spatially varying intensity distortion is investigated. An appropriate similarity measure function that measures the similarity between two images should be robust in the presence of illumination variations. On the other hand, its global minimum correctly represents the parameters of geometrical transform that obtain the perfect alignment of two images. The similarity measure functions of SSD, MI, RC, and our method are obtained between two images (Fig. 4) with respect to the different rotation and translation parameters. Fig. 5 shows the similarity measure functions. It is clear that RISM is robust in the presence of illumination variations. The robustness of RC is also similar to RISM. SSD function does not have a good distinguishable ability to be robust in the

presence of spatially varying intensity distortion. It seems that MI has a good similarity measure, but if geometric transform is nonrigid, MI has a poor performance, which is shown in the simulated data.

B. Simulated Data

Here, we have used the BrainWeb database containing the simulated brain magnetic resonance (MR) data volumes from several protocols, including T1-weighted (MR-T1), T2-weighted (MR-T2), and proton density(MR-PD). We have selected a 2D slice of MR-T1 (218×181), in which its intensities were normalized to $[0, 1]$. To evaluate the proposed similarity measure, we applied geometric and intensity distortion. To generate the moving image, a random perturbation was applied to the corresponding reference image using an FFD. On the other hand, the grid points of FFD are produced by perturbing a uniform grid of points. The grid size was 14×14 and its random perturbation was drawn from a uniform distribution on $[-6, 6]$ interval.

To validate the proposed method, we used two different measures: the transformation root mean square error (RMSE) between the true and estimated transformations: $\varepsilon_{\text{RMSE}} = \sqrt{(1/N) \|T_{\text{true}} - T_{\text{estimated}}\|^2}$ (note that the boundary error influence will not be considered in the transformation RMSE computation), and intensity RMSE between the reference and the clean registered image. To obtain the clean registered image, the estimated geometric transform is applied to the source image without intensity distortion. The mean and standard deviation (SD) of two error measures are calculated by 20 runs of registration in all the experiments. At each run, the intensity distortion and the geometric transform parameters were randomly reinitialized.

1) Experiment 1: Additive Spatially Varying Intensity Distortion: To generate intensity distortion, both reference and moving images are corrupted according to the equation as follows [25]:

- $I(x, y) = I(x, y) + (1/K) \sum_{k=1}^K e^{-(\|x, y - \mu_k\|^2)/(2(30^2))}$
- rescale to $[0, 1]$.

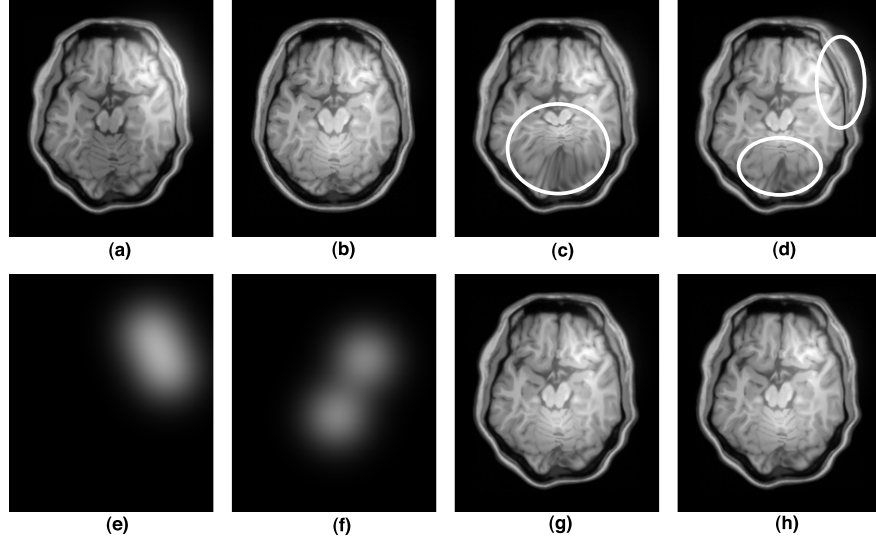


Fig. 6. Experiment 1. We register the floating image (b) onto the reference image (a). (e), (f) Intensity distortion fields added to the reference and floating images, respectively. (a) Reference image. (b) Floating image. (c) SSD result. (d) MI result. (e) Reference bias. (f) Floating bias. (g) RC result. (h) RISM result.

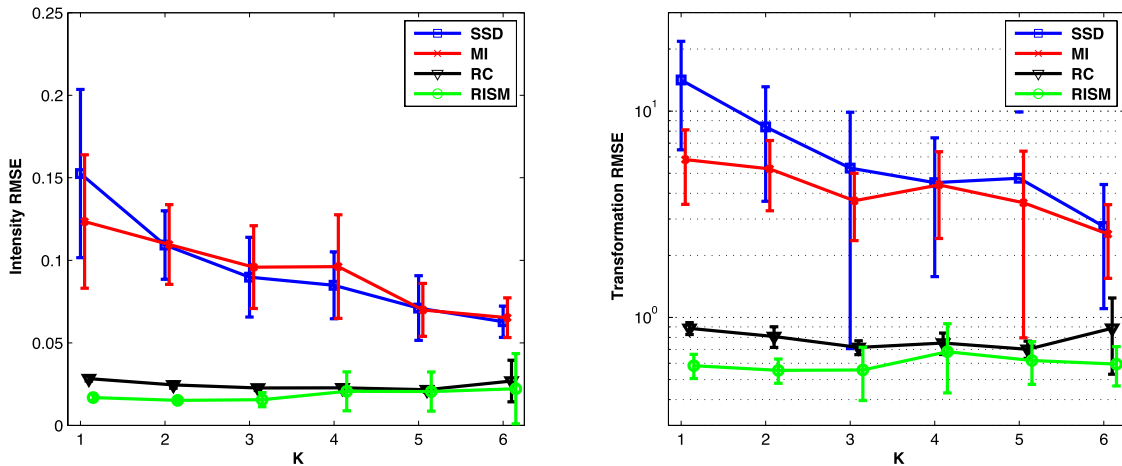


Fig. 7. Registration performances of RISM, RC, SSD, and MI. Both images were corrupted by additive intensity field.

The last term models locally varying intensity field with a mixture of K randomly centered Gaussian functions. The performance accuracy of our method is compared with that of RC, SSD, and MI. An example of the registered images is shown in Fig. 6. These results demonstrate that RISM has accurate performances. RC also obtains a good performance. The performances of SSD and MI are poor, and the registration process failed. We have highlighted the misalignment regions of these approaches with contours in Fig. 6. This may also be seen from the similarity measure functions (Fig. 5). The reason for the poor performance of these similarity measures is clearly because of the global nature of these methods, while here, the intensity distortion is local. Fig. 7 demonstrates the registration performances of RISM, RC, SSD, and MI, for the number K of Gaussian mixture = [1..6]. It can easily be seen that RISM has a better performance with the two measures of validation. From the transformation RMSE point of view, for the cumulative validation of 120 runs (all 20 runs for each K), the mean (standard deviation) registration errors were 0.5983 (0.1524), 0.7917 (0.1723), 6.6371 (6.0024), and 4.2119 (2.2051) for the RISM, RC, SSD,

and MI approaches, respectively. We can see that RISM and RC have subpixel accuracy. As clearly, RISM has significantly better results, and its performance improvement with respect to RC is about 24%.

2) *Experiment 2: Multiplicative Spatially Varying Intensity Distortion:* Similar to experiment 1, this distortion is simulated using the following equation to corrupt images:

$$I(x, y) = I(x, y) \cdot (0.2 + (1/K) \sum_{k=1}^K e^{-(\|x, y - \mu_k\|^2)/(2(30^2))})$$

The results of registration accuracy are shown in Fig. 8. We can see that the results are similar to the results of additive distortion. But in this case, RISM and RC have a similar accuracy, and RISM has no better performance. The reason for this is that in our main model (2), intensity distortion is considered additive, while in this case, it is multiplicative. Nevertheless, our proposed method has a clinically acceptable performance.

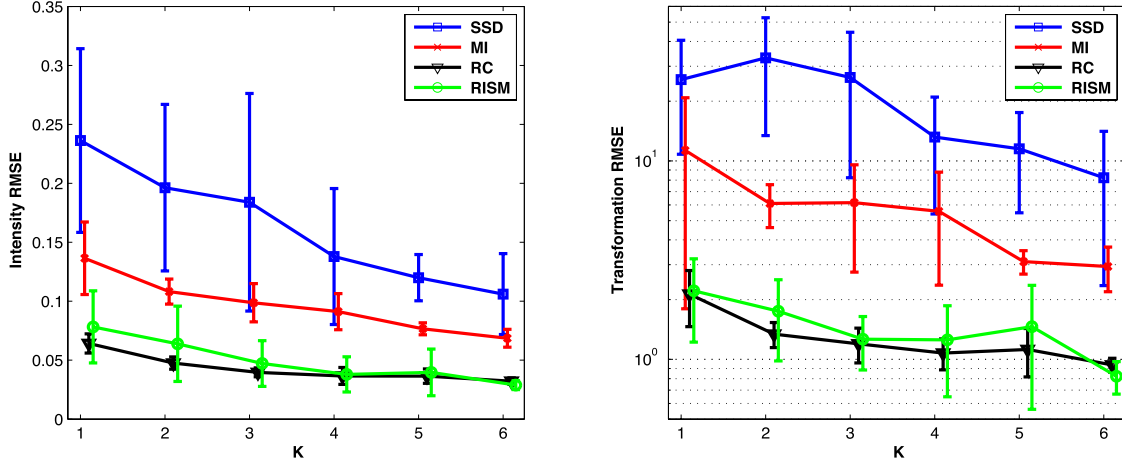


Fig. 8. Registration performances of RISM, RC, SSD, and MI. Both images were corrupted by multiplicative intensity field. In this experiment, to decrease the effect of multiplicative intensity distortion, we did not use any preprocessing method before image registration process.

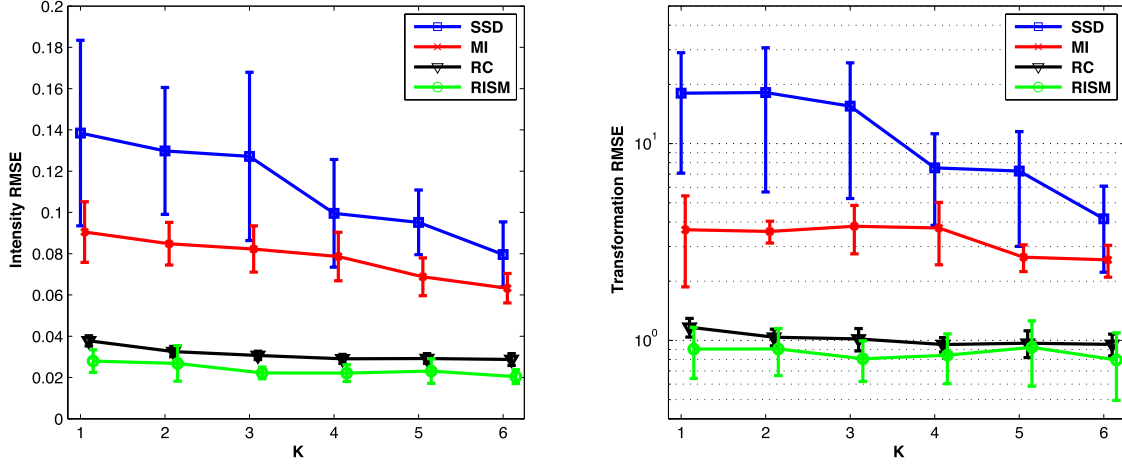


Fig. 9. Registration performances of RISM, RC, SSD, and MI. Both images were corrupted by multiplicative intensity field. In this experiment, to decrease the effect of multiplicative intensity distortion, the simple preprocessing of image enhancement in spatial domain is used by logarithm transform before image registration process.

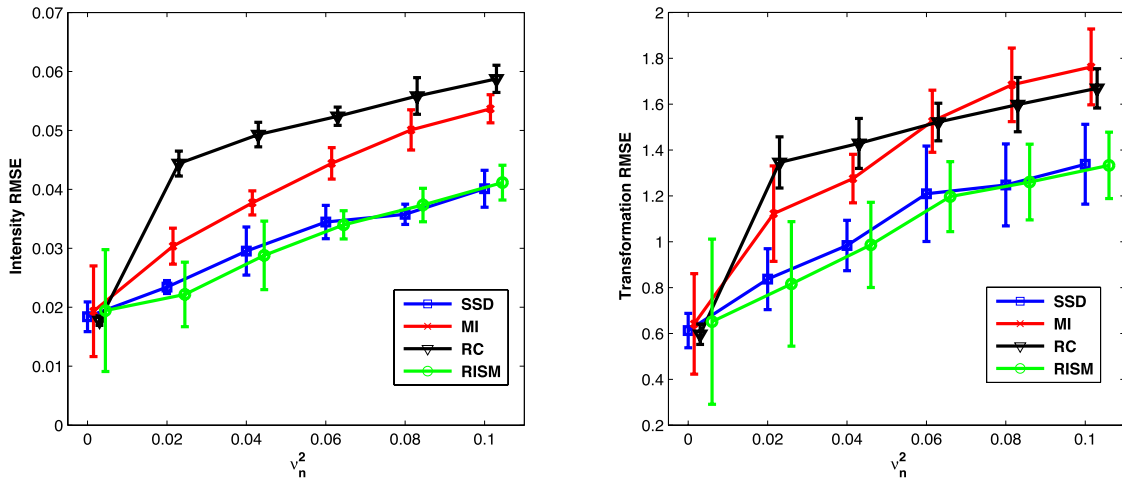


Fig. 10. Registration performances of RISM, RC, SSD, and MI. Floating image was corrupted by the Gaussian noise.

Next, we apply simple preprocessing on the intensities of two images before registration process. Here, to decrease the effect of multiplicative intensity distortion, we used an image enhancement in the spatial domain using the logarithm

transform ($\log(10x + 1)$). The logarithm transform makes conditions of this experiment close to our main model, approximately. Fig. 9 demonstrates the results of registration accuracy of this experiment. It can be seen that the proposed

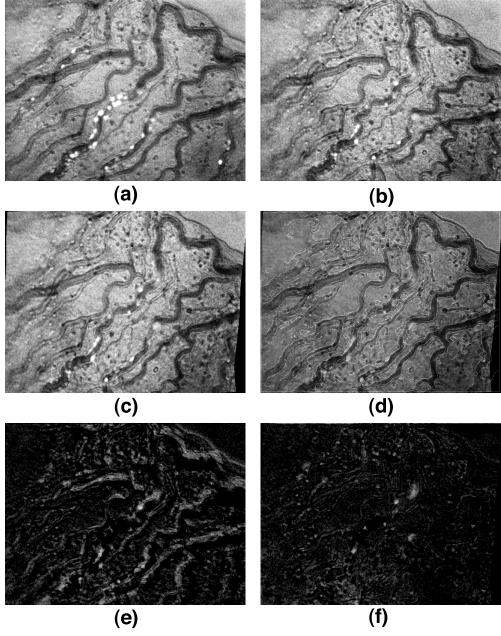


Fig. 11. Iris images: (a) reference image (frame 1); (b) floating image (frame 25); (c) and (d) RISM result and composite view through contour overlap after the registration, respectively; (e) and (f) absolute frame difference before and after registration, respectively.

similarity measure has a better performance by using a simple preprocessing of logarithm transform. From the transformation RMSE point of view, for the cumulative validation of 120 runs (all 20 runs for each K), the mean (standard deviation) registration errors were 0.8622 (0.2610), 1.0167 (0.1387), 11.7763 (9.8367), and 3.3285 (1.1335) for the RISM, RC, SSD, and MI approaches, respectively. It is seen that RC and RISM have superior accuracies in comparison with that of SSD and MI methods. Also, it is clear that RISM has a better performance with subpixel accuracy, and its performance improvement with respect to RC is about 15%.

3) Experiment 3: Additive Gaussian Noise: Here, the proposed similarity is tested in the presence of stationary intensity distortion of Gaussian noise. Floating image is corrupted by additive zero mean Gaussian noise. Fig. 10 shows the results of registration accuracy of this experiment. It can be seen that both methods of RISM and SSD have similar performances. This is because of ℓ_2 norm region (17) in the definition of RISM with respect to the function $f_\gamma(x)$. In fact, when only Gaussian noise is present, and γ is also set to $\sqrt{nmv_n}$, RISM similarity measure is similar to SSD. From Fig. 10, it is clear that the RISM has an accurate and better performance than SSD, MI, and RC in the presence of Gaussian noise.

C. Iris Images

To study immune systems, leukocyte tracking and characterization play the main roles. An important step before tracking leukocytes in an image sequence is motion compensation. A sequence of iris images is useful for tracking leukocytes [46]. The frames of iris sequence have misalignment caused by dilation and contraction of the pupil and head movements during imaging [46], [47]. Note that the motion

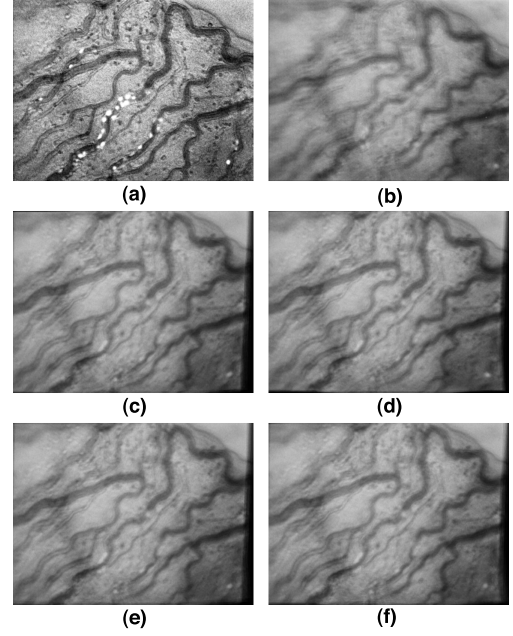


Fig. 12. Iris images: all methods are visually evaluated via the averages of the registered frames. Sharp average image indicates accurate registration result. (a) reference image (frame 1); (b) Average image before registration; (c) Average of SSD results; (d) Average of MI results; (e) Average of RC results; (f) Average of RISM results.

estimation suffers from the presence of noise and intensity variation across the frames. To evaluate the effectiveness of the proposed method, we used a microscopic iris video sequence consisting of 25 frames. We stabilized and rectified these images by nonrigid registration. In this experiment, each frame was registered onto the first frame for the stabilization of the image sequence. Fig. 11 shows an example of the registration result on a pair of image frames. Fig. 11(e) and (f) are the absolute frame difference before and after the registration, respectively. It is seen that the motion artifacts are significantly reduced. Here, we may also visually evaluate all methods in Fig. 12 via the averages of the registered frames obtained using the different similarity measures. Sharp average image indicates accurate registration result. The average image obtained using RISM is clearly sharp, indicating a more accurate registration. The other approaches also have acceptable accuracy. Fig. 13 shows the registration accuracy using the intensity RMSE versus the frame number. We observe that RISM obtained a lower registration error.

D. Dynamic Cardiac MRI

The motion of heart has many information for investigating the heart's architecture and function [48]. To estimate heart's motion, image registration plays a main role. To evaluate the proposed similarity measure, we used a sequence of 2D dynamic cardiac MRI. In this experiment, the next frame was registered onto the previous frame in order to estimate the motion field through time. Fig. 14 shows the registration accuracy via the intensity RMSE versus the frame number. It is seen that RISM has a better performance and achieved lower registration error.

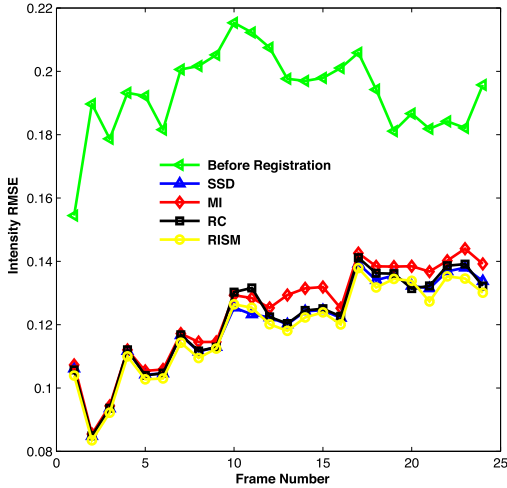


Fig. 13. Registration accuracy: iris sequence is registered frame by frame to stabilize the image sequence.

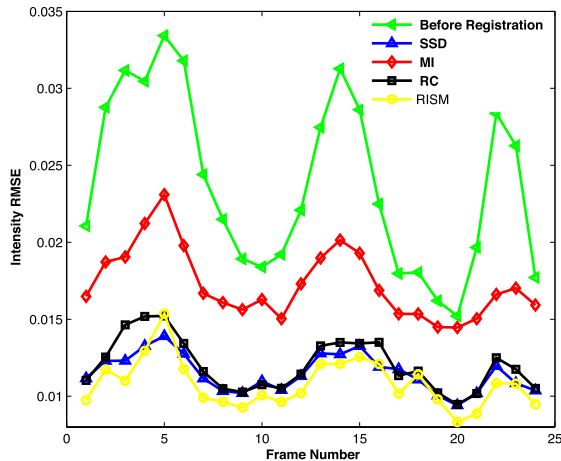


Fig. 14. Registration accuracy: dynamic cardiac MRI is registered frame by frame to estimate the cardiac motion through time.

E. Retina Images

In diseases such as diabetic retinopathy, retina images are frequently used in ophthalmology. These images are usually taken at different times; hence, image registration is needed as an important preprocessing. In these images, distortions such as nonuniform background and blood vessels are present. Hence, registration of retina images is a challenging task. To overcome this problem, feature-based methods are used. Features are the extracted vascular structure or landmarks [49], [50].

Here, we used retina images taken 2 years apart (Fig. 15) [51]. It can be seen from Fig. 15 that there is a strong spatially varying intensity distortion. Traditional similarity measures such as SSD and MI cannot provide a clinically acceptable performance in the presence of this type of distortion. As our similarity measure considers spatially varying intensity distortion via the low-rank model, we expect that this challenge of image registration can be solved by the proposed approach, which is an intensity-based method. Fig. 15 shows the registration results. We obtained a

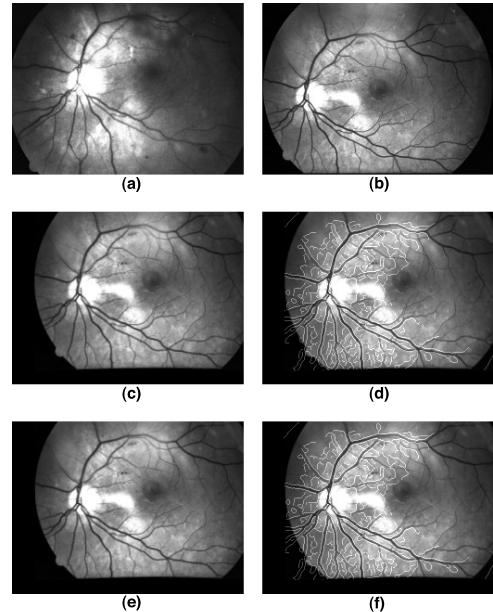


Fig. 15. Retina images taken 2 years apart: (a) reference image; (b) floating image; (c) and (d) RC result and composite view through contour overlap after the registration, respectively; (e) and (f) RISM result and composite view through contour overlap after the registration.

clinically acceptable result using RISM as demonstrated via composite view through contour overlap after the registration. RC also provide an acceptable result.

F. Digital Subtraction Angiography

Digital subtraction angiography (DSA) [52]–[54] is a method of vascular imaging using the contrast agent in the process of X-ray scanning. Blood vessels are highlighted after the injection of the contrast agent and also by removing the background structures. In practice, there are movements caused by breath or patient movement. Hence, motion compensation or image registration is a main preprocessing task in DSA images. Fig. 16 presents one example of real DSA images and the results of different methods. It can be seen that the motion artifacts are significantly reduced after applying the image registration based on RISM. RISM and RC have a better performance than SSD and MI. With respect to the importance of DSA images, one of our future works will especially focus on extending the proposed similarity measure for this application.

G. Real LANDSAT Satellite Images

Image registration is an important preprocess in the application of remote sensing [17]. Registration of multi-date images is a challenging problem. In this experiment, to evaluate the proposed approach we used real LANDSAT images (Fig. 17) captured at different years [55]. It is obvious that illumination variations between images are very large. An acceptable performance of image registration can not be obtained using SSD and MI similarity measures in this example. Our method showed effective and accurate result for these images (Fig. 17). RC also obtained a good performance.

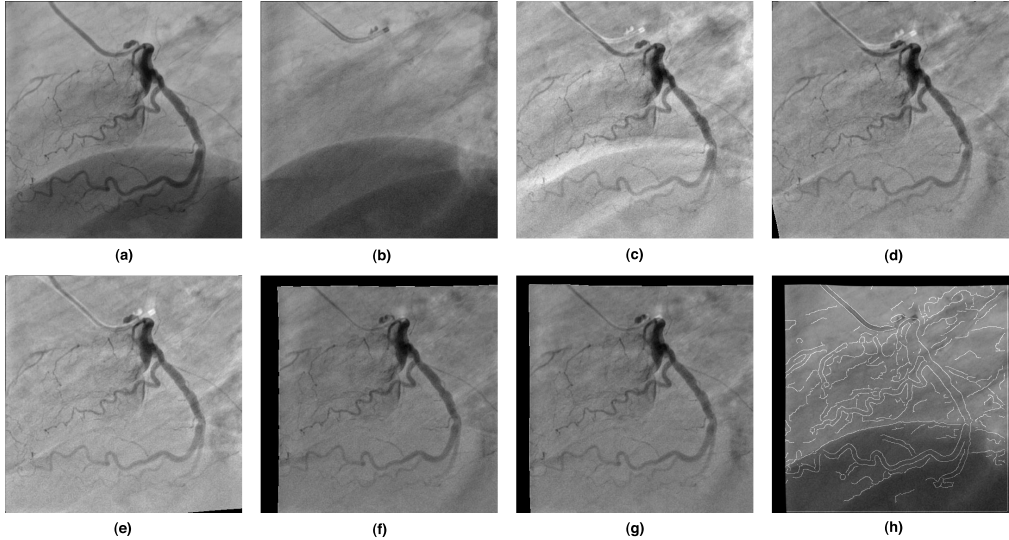


Fig. 16. Registration of coronary angiographic images. (a) Image after the injection of the contrast agent; (b) Image before the injection of the contrast agent; (c) DSA image before registration; (d), (e), (f), and (g) DSA images after the motion compensation using SSD, MI, RC, and RISM, respectively; (g) Composite view of registered background through contour overlap using RISM.

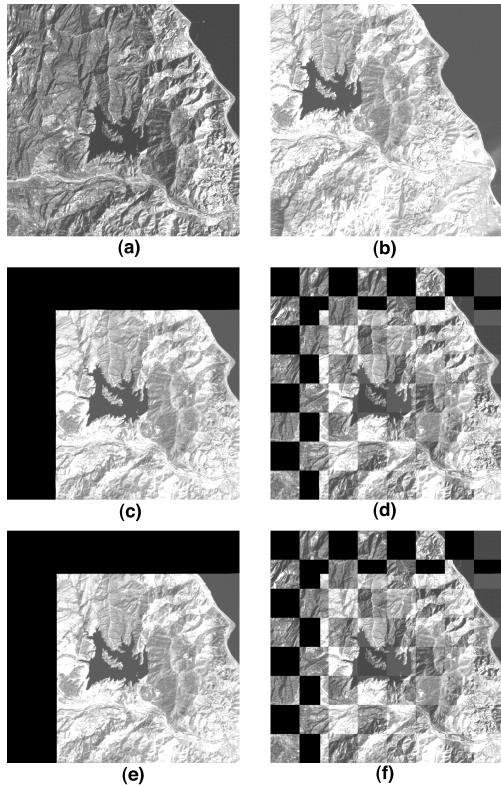


Fig. 17. Real LANDSAT images captured at different years: (a) reference image; (b) floating image; (c) and (d) RC result and composite view after the registration, respectively; (e) and (f) RISM result and composite view after the registration, respectively.

IV. DISCUSSION AND CONCLUSION

In this paper, the low-rank matrix theory is used for defining a new similarity measure. The motivation for this idea is that spatially varying intensity distortion is a low-rank matrix. This consideration is true for medical imaging applications, e.g., Bias field in MRI. Generally, natural images are

of low rank. Considering this, we formulate image registration as the NLLRMD problem. The uniqueness of NLLRMD has been illustrated. The uniqueness theorems are stated based on the intersection of two matrix subspaces. Based on this decomposition, we have used the rank of difference image as an optimal similarity measure in the presence of spatially varying intensity distortion. In fact, image registration and intensity distortion correction are simultaneously achieved with this similarity measure. Considering the Gaussian noise and the effective rank, RISM is introduced as a novel similarity measure. RISM is a combination of rank and SSD. In fact, the proposed similarity measure is a mixture of ℓ_0 and ℓ_2 norms in the domain of singular values of difference image. In this respect, the proposed measure is appropriate in the presence of two model distortions (Gaussian noise and low-rank distortion). The feasibility of the proposed algorithm is also demonstrated on real data. The proposed approach has a better performance than RC, SSD, and MI in the presence of intensity and geometric distortion. Future work will focus on extending our approach to multi-modal image registration.

ACKNOWLEDGEMENT

The authors would like to thank the anonymous reviewers for their fruitful comments and suggestions.

REFERENCES

- [1] R. R. Brooks and S. S. Iyengar, *Multi-Sensor Fusion: Fundamentals and Applications With Software*, Upper Saddle River, NJ, USA: Prentice-Hall, 1998.
- [2] F. Sauer, "Image registration: Enabling technology for image guided surgery and therapy," in *Proc. 27th Annu. Int. Conf. Eng. Med. Biol. Soc.*, Jan. 2006, pp. 7242–7245.
- [3] A. Sotiras, C. Davatzikos, and N. Paragios, "Deformable medical image registration: A survey," *IEEE Trans. Med. Imag.*, vol. 32, no. 7, pp. 1153–1190, Jul. 2013.
- [4] F. P. M. Oliveira and J. M. R. S. Tavares, "Medical image registration: A review," *Comput. Methods Biomed. Eng.*, vol. 17, no. 2, pp. 73–93, 2014.

- [5] A. Ghaffari, R. Khorsandi, and E. Fatemizadeh, "Landmark and intensity based image registration using free form deformation," in *Proc. IEEE EMBS Conf. Biomed. Eng. Sci. (IECBES)*, Dec. 2012, pp. 768–771.
- [6] D. Shen and C. Davatzikos, "HAMMER: Hierarchical attribute matching mechanism for elastic registration," *IEEE Trans. Med. Imag.*, vol. 21, no. 11, pp. 1421–1439, Nov. 2002.
- [7] S. Liao and A. C. S. Chung, "Feature based nonrigid brain MR image registration with symmetric alpha stable filters," *IEEE Trans. Med. Imag.*, vol. 29, no. 1, pp. 106–119, Jan. 2010.
- [8] A. Ghanbari, R. Abbasi-Asl, A. Ghaffari, and E. Fatemizadeh, "Automatic B-spline image registration using histogram-based landmark extraction," in *Proc. IEEE EMBS Conf. Biomed. Eng. Sci. (IECBES)*, Dec. 2012, pp. 1004–1008.
- [9] A. Roche, G. Malandain, X. Pennec, and N. Ayache, "The correlation ratio as a new similarity measure for multimodal image registration," in *Medical Image Computing and Computer-Assisted Intervention* (Lecture Notes in Computer Science), vol. 1496. Berlin, Germany: Springer-Verlag, 1998, pp. 1115–1124.
- [10] W. M. Wells, P. Viola, H. Atsumi, S. Nakajima, and R. Kikinis, "Multi-modal volume registration by maximization of mutual information," *Med. Image Anal.*, vol. 1, no. 1, pp. 35–51, 1996.
- [11] F. Maes, A. Collignon, D. Vandermeulen, G. Marchal, and P. Suetens, "Multimodality image registration by maximization of mutual information," *IEEE Trans. Med. Imag.*, vol. 16, no. 2, pp. 187–198, Apr. 1997.
- [12] A. Roche, X. Pennec, G. Malandain, and N. Ayache, "Rigid registration of 3D ultrasound with MR images: A new approach combining intensity and gradient information," *IEEE Trans. Med. Imag.*, vol. 20, no. 10, pp. 1038–1049, Oct. 2001.
- [13] M. Khader and A. B. Hamza, "Nonrigid image registration using an entropic similarity," *IEEE Trans. Inf. Technol. Biomed.*, vol. 15, no. 5, pp. 681–690, Sep. 2011.
- [14] A. Roche, G. Malandain, and N. Ayache, "Unifying maximum likelihood approaches in medical image registration," INRIA, Rocquencourt, France, Tech. Rep. RR-3741, Jul. 1999.
- [15] C. Studholme, C. Drapaca, B. Iordanova, and V. Cardenas, "Deformation-based mapping of volume change from serial brain MRI in the presence of local tissue contrast change," *IEEE Trans. Med. Imag.*, vol. 25, no. 5, pp. 626–639, May 2006.
- [16] D. L. G. Hill, P. G. Batchelor, M. Holden, and D. J. Hawkes, "Medical image registration," *Phys. Med. Biol.*, vol. 46, no. 3, pp. R1–R45, Mar. 2001.
- [17] M. M. Fouad, R. M. Dansereau, and A. D. Whitehead, "Image registration under illumination variations using region-based confidence weighted M-estimators," *IEEE Trans. Image Process.*, vol. 21, no. 3, pp. 1046–1060, Mar. 2012.
- [18] K. M. Pohl *et al.*, "A unifying approach to registration, segmentation, and intensity correction," in *Medical Image Computing and Computer-Assisted Intervention* (Lecture Notes in Computer Science), vol. 3749. Berlin, Germany: Springer-Verlag, 2005, pp. 310–318.
- [19] K. J. Friston, J. Ashburner, C. D. Frith, J.-B. Poline, J. D. Heather, and R. S. J. Frackowiak, "Spatial registration and normalization of images," *Human Brain Mapping*, vol. 3, no. 3, pp. 165–189, Mar. 1995.
- [20] P. P. Wyatt and J. A. Noble, "MAP MRF joint segmentation and registration of medical images," *Med. Image Anal.*, vol. 7, no. 4, pp. 539–552, 2003.
- [21] A. El-Baz, A. Farag, G. Gimel'farb, and A. E. Abdel-Hakim, "Image alignment using learning prior appearance model," in *Proc. IEEE Int. Conf. Image Process.*, Oct. 2006, pp. 341–344.
- [22] D. Loeckx, P. Slagmolen, F. Maes, D. Vandermeulen, and P. Suetens, "Nonrigid image registration using conditional mutual information," *IEEE Trans. Med. Imag.*, vol. 29, no. 1, pp. 19–29, Jan. 2010.
- [23] X. Zhuang, S. Arridge, D. J. Hawkes, and S. Ourselin, "A nonrigid registration framework using spatially encoded mutual information and free-form deformations," *IEEE Trans. Med. Imag.*, vol. 30, no. 10, pp. 1819–1828, Oct. 2011.
- [24] A. Ghaffari and E. Fatemizadeh, "Sparse-induced similarity measure: Mono-modal image registration via sparse-induced similarity measure," *IET Image Process.*, vol. 8, no. 12, pp. 728–741, 2014.
- [25] A. Myronenko and X. Song, "Intensity-based image registration by minimizing residual complexity," *IEEE Trans. Med. Imag.*, vol. 29, no. 11, pp. 1882–1891, Nov. 2010.
- [26] P. Farnia, A. Ahmadian, T. Shabani, N. D. Serej, and J. Alirezaie, "Brain-shift compensation by non-rigid registration of intra-operative ultrasound images with preoperative MR images based on residual complexity," *Int. J. Comput. Assist. Radiol. Surgery*, vol. 10, no. 5, pp. 555–562, 2015.
- [27] Z. Liu and L. Vandenberghe, "Interior-point method for nuclear norm approximation with application to system identification," *SIAM J. Matrix Anal. Appl.*, vol. 31, no. 3, pp. 1235–1256, 2009.
- [28] B. Recht, M. Fazel, and P. A. Parrilo, "Guaranteed minimum-rank solutions of linear matrix equations via nuclear norm minimization," *SIAM Rev.*, vol. 52, no. 3, pp. 471–501, 2010.
- [29] E. J. Candès and B. Recht, "Exact matrix completion via convex optimization," *Found. Comput. Math.*, vol. 9, no. 6, pp. 717–772, 2009.
- [30] Y. Peng, A. Ganesh, J. Wright, W. Xu, and Y. Ma, "RASL: Robust alignment by sparse and low-rank decomposition for linearly correlated images," in *Proc. IEEE Conf. Comput. Vis. Pattern Recognit. (CVPR)*, Jul. 2010, pp. 763–770.
- [31] V. Hamy *et al.*, "Respiratory motion correction in dynamic MRI using robust data decomposition registration—Application to DCE-MRI," *Med. Image Anal.*, vol. 18, no. 2, pp. 301–313, 2014.
- [32] C. Eckart and G. Young, "The approximation of one matrix by another of lower rank," *Psychometrika*, vol. 1, no. 3, pp. 211–218, 1936.
- [33] L. Mirsky, "Symmetric gauge functions and unitarily invariant norms," *Quart. J. Math.*, vol. 11, no. 1, pp. 50–59, 1960.
- [34] G. Marsaglia and G. P. Styan, "When does $\text{rank}(A + B) = \text{rank}(A) + \text{rank}(B)$?" *Can. Math. Bull.*, vol. 15, no. 3, pp. 451–452, 1972.
- [35] K. Konstantinides and K. Yao, "Statistical analysis of effective singular values in matrix rank determination," *IEEE Trans. Acoust., Speech, Signal Process.*, vol. 36, no. 5, pp. 757–763, May 1988.
- [36] E. J. Candès and T. Tao, "Near-optimal signal recovery from random projections: Universal encoding strategies?" *IEEE Trans. Inf. Theory*, vol. 52, no. 12, pp. 5406–5425, Dec. 2006.
- [37] P. J. Huber, *Robust Statistics*. New York, NY, USA: Springer-Verlag, 2011.
- [38] G. Mohimani, M. Babaie-Zadeh, and C. Jutten, "A fast approach for overcomplete sparse decomposition based on smoothed ℓ^0 norm," *IEEE Trans. Signal Process.*, vol. 57, no. 1, pp. 289–301, Jan. 2009.
- [39] A. Ghaffari, M. Babaie-Zadeh, and C. Jutten, "Sparse decomposition of two dimensional signals," in *Proc. IEEE Int. Conf. Acoust., Speech Signal Process. (ICASSP)*, Apr. 2009, pp. 3157–3160.
- [40] H. Ghasemi, M. Malek-Mohammadi, M. Babaie-Zadeh, and C. Jutten, "SRF: Matrix completion based on smoothed rank function," in *Proc. IEEE Int. Conf. Acoust., Speech Signal Process. (ICASSP)*, May 2011, pp. 3672–3675.
- [41] M. Malek-Mohammadi, M. Babaie-Zadeh, A. Amini, and C. Jutten, "Recovery of low-rank matrices under affine constraints via a smoothed rank function," *IEEE Trans. Signal Process.*, vol. 62, no. 4, pp. 981–992, Feb. 2014.
- [42] D. L. Donoho and J. M. Johnstone, "Ideal spatial adaptation by wavelet shrinkage," *Biometrika*, vol. 81, no. 3, pp. 425–455, 1994.
- [43] A. S. Lewis, "The convex analysis of unitarily invariant matrix functions," *J. Convex Anal.*, vol. 2, no. 1, pp. 173–183, 1995.
- [44] D. Rueckert, L. I. Sonoda, C. Hayes, D. L. G. Hill, M. O. Leach, and D. J. Hawkes, "Nonrigid registration using free-form deformations: Application to breast MR images," *IEEE Trans. Image Process.*, vol. 18, no. 8, pp. 712–721, Aug. 1999.
- [45] [Online]. Available: <http://www.bic.mni.mcgill.ca/brainweb/>
- [46] X. B. Song, A. Myronenko, S. R. Plank, and J. T. Rosenbaum, "Registration of microscopic iris image sequences using probabilistic mesh," in *Medical Image Computing and Computer-Assisted Intervention*. Berlin, Germany: Springer-Verlag, 2006, pp. 553–560.
- [47] Y. Peng, A. Ganesh, J. Wright, W. Xu, and Y. Ma, "RASL: Robust alignment by sparse and low-rank decomposition for linearly correlated images," *IEEE Trans. Pattern Anal. Mach. Intell.*, vol. 34, no. 11, pp. 2233–2246, Jul. 2012.
- [48] X. Papademetris, A. J. Sinusas, D. P. Dione, R. T. Constable, and J. S. Duncan, "Estimation of 3D left ventricular deformation from medical images using biomechanical models," *IEEE Trans. Med. Imag.*, vol. 21, no. 7, pp. 786–800, Jul. 2002.
- [49] Z. Ghassabi, J. Shanbehzadeh, A. Sedaghat, and E. Fatemizadeh, "An efficient approach for robust multimodal retinal image registration based on UR-SIFT features and PIIFD descriptors," *EURASIP J. Image Video Process.*, vol. 2013, no. 1, pp. 1–16, 2013.
- [50] C. V. Stewart, C.-L. Tsai, and B. Roysam, "The dual-bootstrap iterative closest point algorithm with application to retinal image registration," *IEEE Trans. Med. Imag.*, vol. 22, no. 11, pp. 1379–1394, Nov. 2003.
- [51] F. Zana, I. Meunier, and J. C. Klein, "A region merging algorithm using mathematical morphology: Application to macula detection," in *Proc. ISMM*, 1998, pp. 423–430.
- [52] W. R. Brody, "Digital subtraction angiography," *IEEE Trans. Nucl. Sci.*, vol. 29, no. 3, pp. 1176–1180, Jun. 1982.

- [53] M. Nejati, S. Sadri, and R. Amirfattahi, "Nonrigid image registration in digital subtraction angiography using multilevel B-spline," *BioMed Res. Int.*, vol. 2013, Jun. 2013, Art. ID 236315.
- [54] B. Liu, Q. Zhao, J. Dong, X. Jia, and Z. Yue, "A stretching transform-based automatic nonrigid registration system for cerebrovascular digital subtraction angiography images," *Int. J. Imag. Syst. Technol.*, vol. 23, no. 2, pp. 171–187, 2013.
- [55] [Online]. Available: <http://vision.ece.ucsb.edu/registration/satellite/>



Aboozar Ghaffari received the B.Sc. degree in electrical engineering from the Shahid Bahonar University of Kerman, Iran, in 2006, and the M.Sc. and Ph.D. degrees in electrical engineering from the Sharif University of Technology, Tehran, Iran, in 2009 and 2015, respectively.

His main research areas are medical image processing, pattern recognition, sparse signal processing, statistical Signal processing, and machine learning for signal processing.



Emad Fatemizadeh (M'95) received the Ph.D. degree from Tehran University, Tehran, Iran. He has been a Biomedical Engineering Faculty Member with the Department of Electrical Engineering, Sharif University of Technology, Tehran, since 2004. His current research interests include biomedical engineering, such as medical image analysis and processing, bioinformatics, statistical pattern recognition, medical data mining, and machine learning.

Dr. Fatemizadeh is a member of the Board of Founders of the Iranian Society of Machine Vision and Image Processing.